ELSEVIER

Journal of Non-Crystalline Solids 220 (1997) 267–279

JOURNAL OF NON-CRYSTALLINE SOLIDS

XPS and magnetization studies of cobalt sodium silicate glasses

A. Mekki [a,b], D. Holland [a,*], Kh. Ziq [b], C.F. McConville [a]

[a] *Department of Physics, University of Warwick, Coventry CV4 7AL, UK*
[b] *Department of Physics, KFUPM, Dhahran 31261, Saudi Arabia*

Received 20 November 1996; revised 14 April 1997

Abstract

Cobalt sodium silicate glasses with the chemical composition $(0.70 - x)SiO_2$–$(0.30)Na_2O$–$xCoO$, where $0.0 \leq x \leq 0.20$, have been investigated by means of X-ray photoelectron spectroscopy (XPS) and magnetization techniques. The Co 2p spectra show intense satellite structures ~ 6 eV above the photoelectron peak and the Co $2p_{3/2}$–Co $2p_{1/2}$ separation was ~ 15.9 eV for all the samples studied. These observations indicate the presence of high spin Co^{2+} ions in the glasses. The Co 3p spectra have been fitted with contributions from octahedral and tetrahedral Co^{2+} and the ratio $[Co^{2+}(oct)]/[Co^{2+}_{Total}]$ increases with increasing CoO content. The O 1s spectra also show composition-dependent changes. The fraction of non-bridging oxygen atoms was determined from these spectra and was found to increase with increasing cobalt oxide. Co(II) ions are found to be incorporated in the glass as network modifiers but the contribution from SiOCo(II) to the non-bridging part of the O 1s signal could be separated from that from SiONa by simulating the spectrum. DC magnetic susceptibility measurements were performed on the same samples but these suggest that Co^{2+} exists mainly in octahedral coordination. The magnetic data indicate that the exchange interaction is antiferromagnetic and increases with increasing CoO in the glass. © 1997 Published by Elsevier Science B.V.

1. Introduction

In recent years there have been several examples where X-ray photoelectron spectroscopy (XPS) has been used to study the electronic structure and spectral properties of transition metal oxides [1,2]. In particular, XPS has been used to measure the so called chemical shifts associated with core level photoemission spectra, when non-equivalent atoms of the same element in a solid give rise to core level peaks with measurably different binding energies. Photoionization of transition metal compounds also gives rise to other secondary features in the XPS spectra, such as multiplet splitting and shake-up satellite structures accompanying the main photoelectron spectral lines [3]. These secondary XPS features are present only when transition metal ions have unpaired electrons in the outer shell. For example, in Cu^{2+} containing compounds ($3d^9$ configuration), strong satellites are observed associated with the Cu $2p_{3/2}$ and Cu $2p_{1/2}$ core levels, while in Cu^+ ($3d^{10}$ configuration) containing compounds, no such satellite structure is observed experimentally or as a result of model calculations [4].

XPS has also proved to be a useful tool for investigating the structure of oxide glasses [5]. For example, using XPS it is possible to differentiate between bridging and non-bridging oxygen atoms in the glass structure. This approach has been success-

* Corresponding author. Tel.: +44-1203 523 396; fax: +44-1203 692 016; e-mail: phsay@csv.warwick.ac.uk.

PII S0022-3093(97)00300-1

fully applied to several binary glasses [6–8] as well as several more complex systems [9–12]. Satellite structures associated with their 2p core level peaks have been observed when individual transition metals have been introduced into oxide glasses. These have been used qualitatively to identify the oxidation state of the transition metals in glasses [13]. Recently, XPS has been used successfully to determine the content of different oxidation states of transition metals in oxide glasses, such as iron and copper in sodium silicate glass [14–17].

In the present work, cobalt oxide was selected for addition to a sodium silicate base glass for a variety of reasons. Firstly, it has magnetic and catalytic properties that are of considerable technological importance [18,19]. Furthermore, Co shows prominent satellite structures in XPS and can exist in different oxidation states and coordinations in oxide glasses. In the present paper, we report the results of an XPS and magnetization study following the introduction of various amounts of CoO, up to a nominal 20 mol%, into a sodium silicate base glass. The aim was to measure the non-bridging oxygen content, investigate the redox state of the cobalt and to identify the different bonding coordinations of cobalt ions in these glasses.

2. Experimental details

2.1. Sample preparation

The glass samples were prepared using commercially available, analytical grade powders of $CoCO_3$ (for CoO), Na_2CO_3 (for Na_2O) and SiO_2. Calculated amounts of these powders were mixed and melted in 95%Pt/5%Rh crucibles at 1400°C for 2 h. The glass, obtained by quenching the liquid into deionised water, was crushed and then remelted at the same temperature to improve the homogeneity of the glass. This final liquid was then cast into preshaped, graphite-coated steel moulds, yielding rod specimens with dimensions $6 \times 6 \times 30$ mm^3. After casting, the specimens were transferred to another furnace maintained at 50°C below the glass transition temperature T_g, determined from differential thermal analysis (DTA), for 2 h and then cooled to room temperature at a rate of 30°C/h. X-ray powder diffraction analysis indicated that the samples thus formed were completely amorphous. After preparation, the samples were stored in a desiccator.

Table 1
Composition of the prepared and analyzed cobalt sodium silicate glasses. The relative uncertainty in the ICP data is about ±5%

x	Nominal			Analyzed		
	Na_2O	SiO_2	CoO	Na_2O	SiO_2	CoO
0.0	0.30	0.70	0.0	0.306	0.694	0.0
0.043	0.30	0.65	0.05	0.299	0.655	0.043
0.086	0.30	0.60	0.10	0.303	0.61	0.086
0.132	0.30	0.55	0.15	0.313	0.556	0.132
0.186	0.30	0.50	0.20	0.306	0.51	0.186

Chemical compositions were determined by inductively-coupled-plasma, emission spectroscopy (ICP). Each composition was analyzed at least twice and the estimated relative uncertainty in the technique is ±5%. Table 1 lists the batch and the analyzed glass compositions.

2.2. XPS measurements

The experiments were carried out in a spectrometer (VG Scientific ESCALAB Mk II) equipped with a dual aluminum–magnesium anode X-ray gun and a 150 mm concentric hemispherical analyzer. Photoelectron spectra from C 1s, O 1s, Co 2p, Co 3p, Na 1s and Si 2p core levels were recorded using a computer controlled data collection system described elsewhere [20]. X-ray photoemission measurements were performed using non-monochromatic Al Kα (1486.6 eV) radiation from an anode operated at 130 W. The energy scale of the spectrometer was calibrated with Cu $2p_{3/2} = 932.67$ eV, Cu $3p_{3/2} = 74.9$ eV and Au $4f_{7/2} = 83.98$ eV photoelectron lines. The electron energy analyzer was operated with a pass energy of 10 eV for the high resolution XPS studies (the analyzer energy resolution is 0.9 eV), whereas a pass energy of 50 eV was used for routine survey scans.

For XPS measurements, a glass rod from each composition was fractured in ultra high vacuum (UHV), where the base pressure in the analysis chamber was routinely $< 2 \times 10^{-10}$ mbar. Prior to introduction into the vacuum, the glass bars were notched to guide the fracture, yielding flat uncontaminated surfaces. Fracturing in UHV is considered to be the optimum method of producing a clean surface

most representative of the bulk structure. Any other surface treatment (such as ion bombardment) changes composition and chemical states, especially relating to the alkali ion distribution [21]. For consistency, all binding energies are reported with reference to the C 1s transition at 284.6 eV ± 0.2 eV which arises from minor hydrocarbon contaminants in the vacuum and is generally accepted to be independent of the chemical state of the sample under investigation.

All of the spectra presented in this paper have been corrected for the charging effect and the presence of any inelastic background. The O 1s and Co 3p spectra were smoothed and fitted with the weighted sum of two Gaussian–Lorentzian curves (G–L ratio = 30%) representing bridging and non-bridging oxygen, and the possible cobalt bonding coordinations and/or oxidation states, respectively. The Lorentzian component of the fitted spectrum arises from the natural peak shape, while the Gaussian component represents the instrumental broadening contribution to the spectrum. A non-linear, least-squares algorithm was used to find each best fit solution, varying areas, binding energies and full-width, half maxima of the peaks. The fraction of non-bridging oxygens and Co^{2+}(oct) were determined from the respective area ratios. More than one sample of each glass composition was analyzed in this manner and the overall accuracy in the determination of the peak position and chemical shift was ≤ 0.2 eV. The quantitative oxygen bonding results (based on relative peak areas) and cobalt redox analysis were reproducible to ±5% and ±10%, respectively. A period of approximately 2 h was required to collect the necessary data set for each sample and, during this time, there was no evidence of any X-ray induced reduction of the cobalt in the glass.

2.3. Glass properties

Several properties of each glass sample were measured. Glass transition temperatures were measured using DTA (heating rate 10°C m^{-1}), and thermal expansion coefficients (α) were determined in the range from room temperature to 400°C using dilatometry and a heating rate of 5°C m^{-1}. The thermal expansion coefficient was measured relative to that of silica and a correction factor applied [22]. The density of each glass was also measured using Archimedes' principle. The sample was weighed in air, and then in degassed, distilled water.

2.4. Magnetic measurements

The magnetization data (M vs. H and M vs. T) were recorded using a computer-controlled, variable-temperature, vibrating sample magnetometer (VSM) (PAR/Lake Shore 4500/150A) incorporating a 9 Tesla superconducting magnet and a temperature controller, capable of temperature control in the range 2 to 300 K. The temperature measuring sensor was a calibrated carbon glass resistor located near the specimen and the system was calibrated using a pure nickel standard. The overall accuracy in the temperature measurements was better than 1% throughout the range, while that of the magnetization measurements was estimated to be approximately ±5%.

3. Results

Wide scan X-ray photoelectron spectra, in the binding energy range 0 to 1200 eV, for each of the

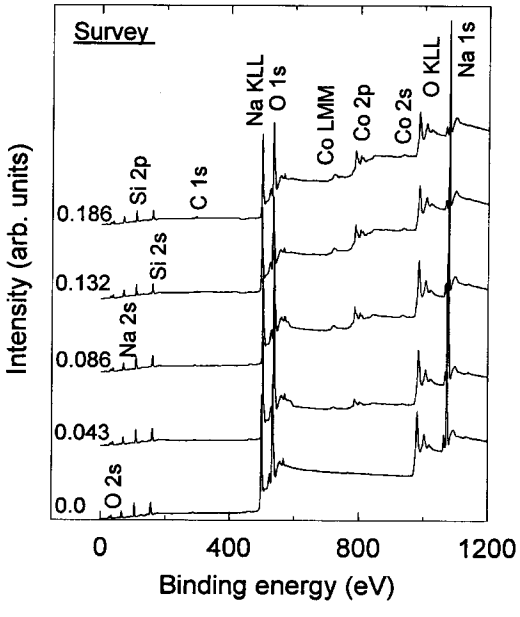

Fig. 1. XPS wide scans of the fractured cobalt sodium silicate glass surfaces with increasing cobalt oxide content.

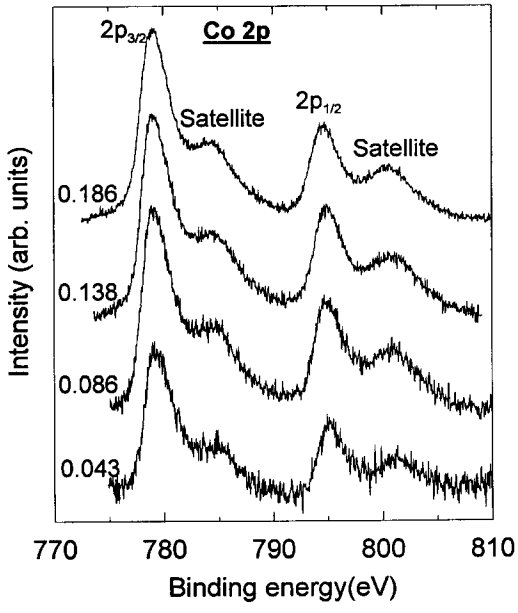

Fig. 2. High resolution Co 2p spectra for glasses containing 4 to 18.6 mol% CoO.

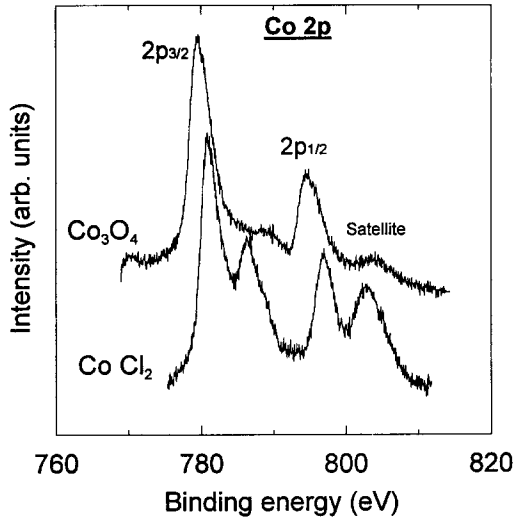

Fig. 3. High resolution Co 2p spectra for $CoCl_2$ and Co_3O_4 compounds. Note the different peak positions and satellite structures.

glass samples investigated, are shown in Fig. 1. The XPS and Auger lines from the constituent elements in the glass are easily identified and marked on the spectra. A high resolution spectrum, taken in the binding energy range 280 to 300 eV, revealed the existence of a small, single C 1s peak which was used as an energy reference at 284.6 eV ± 0.2 eV. The C 1s peak associated with any carbonates (such as Na_2CO_3) has a higher binding energy of 289.3 eV and this peak was not observed in any of the recorded spectra.

3.1. Cobalt spectra

A high resolution XPS scan in the binding energy region 770 to 810 eV is shown in Fig. 2. The peaks at binding energies ~780 eV and ~796 eV are attributed to core level transitions arising from the spin–orbit doublet of the Co 2p. Strong satellite features at ~6 eV on the higher binding energy side of the main peak are also observed for all the cobalt doped glass samples. Spectra of $CoCl_2$ and Co_3O_4 are also shown in Fig. 3 for comparison. As can be seen, the Co 2p spectrum in $CoCl_2$ shows a satellite

Table 2
Binding energies for the Co 2p core level spectra and their corresponding satellites. ΔE represents the energy separation between the Co $2p_{3/2}$ and Co $2p_{1/2}$

x	Co $2p_{3/2}$ (eV ± 0.2)	Sat. $2p_{3/2}$ (eV ± 0.2)	Co $2p_{1/2}$ (eV ± 0.2)	Sat. $2p_{1/2}$ (eV ± 0.2)	$\Delta E_{3/2-1/2}$ (eV ± 0.2)
0.043	780.1	785.7	796.1	802.6	16.0
0.086	780.2	785.8	796.2	802.7	15.9
0.132	780.0	785.4	795.9	802.1	15.9
0.186	780.1	785.7	795.9	802.2	15.8
CoO [a]	780.5	786.4	796.3	803.0	15.8
$CoCl_2$	780.8	786.5	796.8	803.0	16.0
Co_3O_4	779.6	789.5	794.5	804.5	14.9

[a] Taken from Ref. [24].

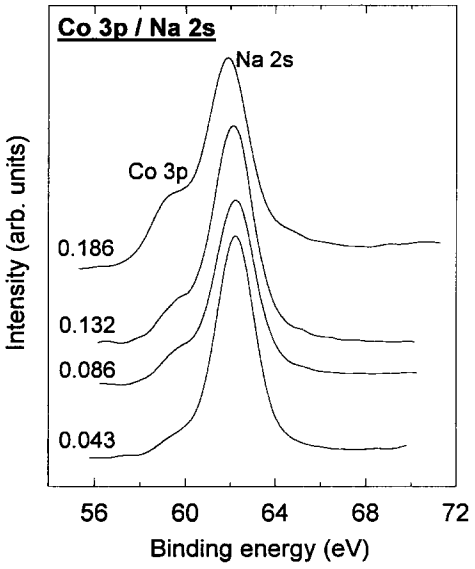

Fig. 4. High resolution Co 3p/Na 2s spectra for the analyzed glass samples.

structure similar to that observed in the glass samples, while the same satellites are smaller in the Co 2p spectrum of the Co_3O_4 compound. It can be seen, from Table 2 and Figs. 2 and 3, that the Co $2p_{3/2}$–Co $2p_{1/2}$ separation in the glasses is similar to that in $CoCl_2$, while it is less in the Co_3O_4 powder. However, the peak width of the Co 2p spectra and their corresponding satellites are narrower in the $CoCl_2$ and Co_3O_4 compounds than in the glass samples. This difference indicates that cobalt in the glass samples exists in either more than one oxidation state or more than one coordination geometry. It was not possible, however, to resolve the Co 2p spectra due to the width of the lines and their satellites. Hence, in order to quantify the valence state and/or the different coordinations of cobalt in the glass samples, it was necessary to analyze the Co 3p core-level transition, which overlaps slightly with the Na 2s line. The Co 3s line did not overlap with any of the other photoelectron lines but was too broad and too small to analyze with any confidence. The Co 3p/Na 2s spectra for the glass samples are shown in Fig. 4.

3.2. O 1s spectra

The O 1s photoelectron core level spectra are shown in Fig. 5 for the base glass, as well as the cobalt doped glass samples, and three resolved peaks can be observed in each spectrum. As cobalt oxide is increased, the smallest binding energy peak increases with respect to the peak with a binding energy of ~ 532 eV, while the largest binding energy peak remains the same in all the glass samples. This latter peak is attributed to the Na KLL Auger transition. In the case of the base sodium silicate glass, it is known that the incorporation of Na_2O breaks the tetrahedral bonds of the SiO_2 and forms bonds of the type SiO^-Na^+ in the glass network. The oxygen atoms linked covalently to two silicons are referred to as bridging oxygen atoms (BO), while those joined covalently to one silicon and ionically to one sodium are termed non-bridging oxygen atoms (NBO).

3.3. Si 2p and Na 1s core level spectra

Both the Si 2p and Na 1s photoelectron core level spectra were measured for all the glass samples investigated. The measured binding energies, as well as the corresponding peak full widths at half maximum (FWHM) are reported in Table 5. As can be seen from these data, as more cobalt is introduced into the base glass, the peak position of the Si 2p peak shifts to lower binding energies by a total of ~ 1 eV over the cobalt oxide concentration range

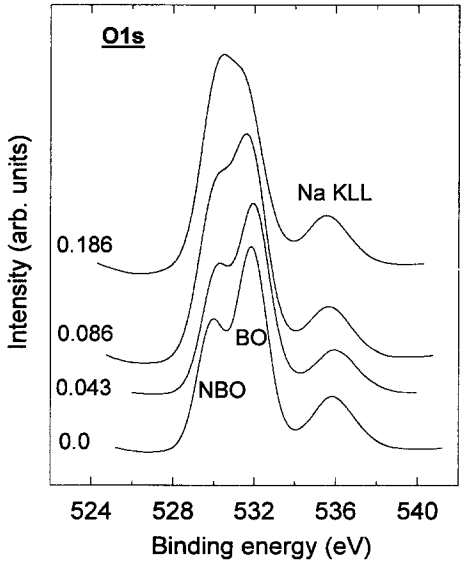

Fig. 5. High resolution O 1s transition for the analyzed glass samples.

studied. Similar behaviour has also been observed when increasing amounts of Fe_2O_3 are added to the same sodium silicate base glass [14]. There is also a small shift, about 0.4 eV toward lower binding energies, for the Na 1s core level line, as shown in Table 5 and the peaks are symmetric with a FWHM of ~ 2.2 eV suggesting that sodium exists in only one bonding configuration in these glasses.

3.4. Physical properties

The results of the glass transition temperature (T_g), density (ρ) and thermal expansion coefficient (α) measurements on these glasses are shown, in Fig. 6a–c respectively, as a function of the cobalt oxide content in the glass. The glass density increases while the glass transition decreases with increasing CoO content. The thermal expansion coefficient, measured over the range of room temperature to 300°C, initially decreases with increasing CoO but appears to reach a constant value at ~ 12.8 mol% CoO. Similar behaviour for α was also observed when Fe_2O_3 was substituted in increasing amounts for SiO_2 in sodium silicate glasses [14].

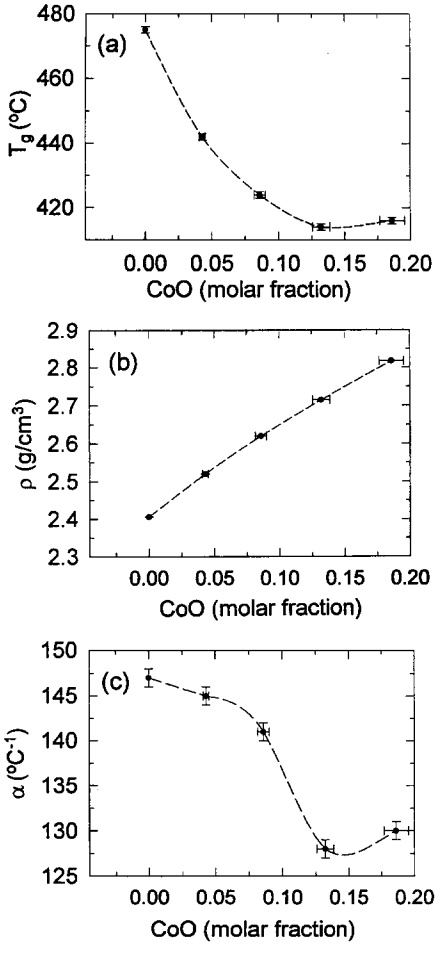

Fig. 6. Variations of (a) glass transition temperature, (b) density and (c) thermal expansion coefficient with CoO content in the glass samples. The dotted lines are drawn to guide the eye.

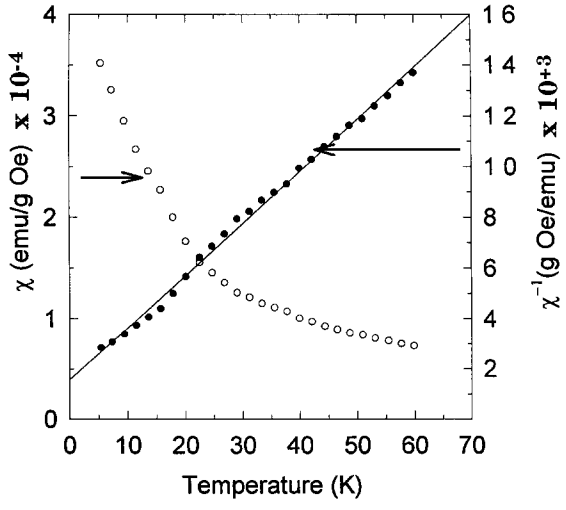

Fig. 7. DC magnetic susceptibility for the $x = 0.086$ glass as plots of χ vs. T and χ^{-1} vs. T. The solid line represents the Curie–Weiss law.

3.5. Magnetic susceptibility and M versus H data

The DC magnetic susceptibility (χ) data for the 0.086 CoO doped glass, and its inverse (χ^{-1}), are shown in Fig. 7 as a function of temperature over the range 2 to 60 K. The data in Fig. 8 shows χ^{-1} versus T for all the cobalt doped glass samples investigated. As can be seen, the high temperature susceptibility follows a Curie–Weiss law; $\chi = C/(T - \theta)$ with a negative Curie temperature which implies that the cobalt ion–ion interaction is antiferromagnetic [30]. The magnetic parameters deduced from the data are summarized in Table 6. The Curie constant and the Curie temperature increases, while the effective magnetic moment (μ_{eff}) decreases with increasing cobalt oxide content in the glass. The Curie temperature is negative, indicating antiferro-

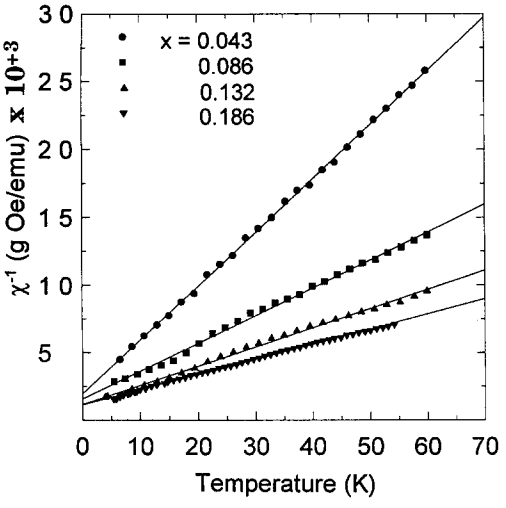

Fig. 8. DC magnetic susceptibility for all the glass samples investigated. The solid lines represent the Curie–Weiss law.

magnetic interaction which increases with increasing CoO content in the glass. The effect of the exchange interaction can be seen graphically by plotting M versus H/T. Magnetic measurements were performed at more than four temperatures for each sample making it possible to represent the magnetization data as a function of H/T. Fig. 9a–d show all the data for all the samples studied and it can be seen that the spread of the data on the H/T scale increases with increase in CoO in the sample. These data further confirm that the exchange interaction, between the magnetic ions, increases with increasing CoO content in the glass.

4. Discussion

4.1. XPS results

Previous studies have been carried out on a number of cobalt compounds and complexes [1,23,24]. In those studies, the analysis of the cobalt photoelectron spectra was made difficult by the fact that cobalt can exist in different oxidation states, different coordination geometries and different spin states for the same

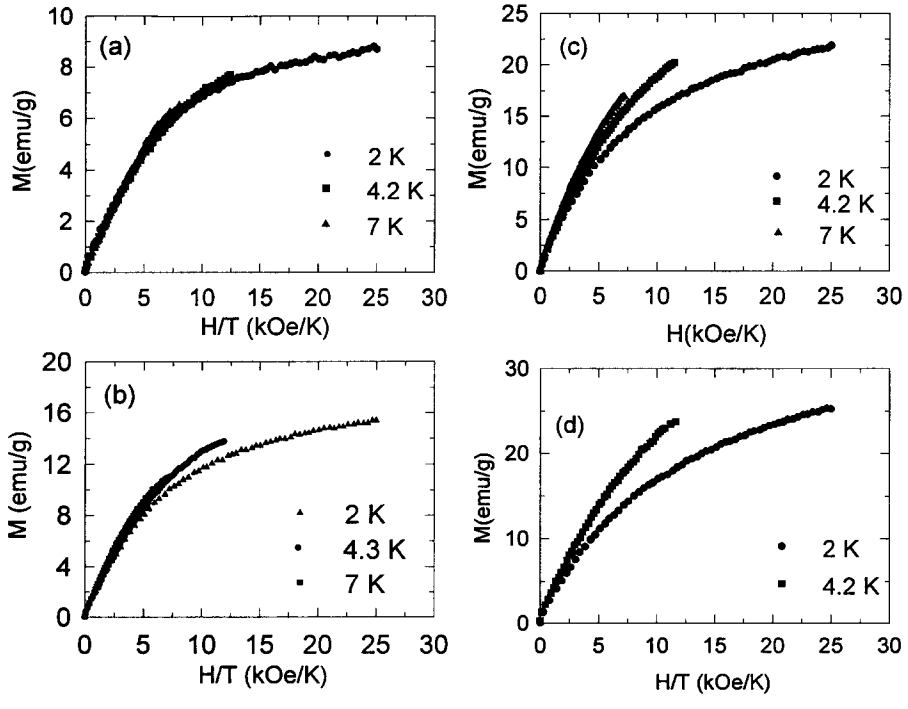

Fig. 9. Magnetization vs. H/T at different temperatures for the glass series: (a) $x = 0.043$, (b) $x = 0.086$, (c) $x = 0.132$, and (d) $x = 0.186$.

oxidation state. Intense satellite structures have been observed for Co 2p spectra, about 5–6 eV above the Co $2p_{3/2}$ and the Co $2p_{1/2}$ transitions, in the case of high-spin Co^{2+} ($S = 3/2$) compounds (such as $CoCl_2$, see Fig. 3), whereas these satellites are very weak, and located about 10 eV above the core level lines, for compounds containing low-spin, diamagnetic Co^{3+} ($S = 0$), such as Co_3O_4, where Co^{3+} is predominant (see Fig. 3). The intensities of the satellites are larger in the high-spin Co^{2+} than in the low-spin Co^{2+} ($S = 1/2$) compounds and complexes [3]. This effect was investigated by Briggs and Gibson [23] who reported measurements on cobalt complexes and observed that the Co $2p_{3/2}$–Co $2p_{1/2}$ separation increased with the number of unpaired electrons. Hence, the peak separation between the spin-orbit Co 2p spectra for complexes with $S = 3/2 > S = 1/2 > S = 0$. This change in the doublet separation is due to the exchange splitting of the 2p levels by the unpaired valence electrons [3]. In these cobalt complexes, it was found that this separation was 15.0 eV for diamagnetic Co^{3+}, 15.4 eV for low-spin Co^{2+} and 16.0 eV for high-spin Co^{2+} ions. It was also found, in other studies [25], that the Co $2p_{3/2}$ photoelectron transition for compounds containing only Co^{3+} was detected ~ 0.9 eV *lower* than that of compounds containing only Co^{2+}. This decrease seems to be due to a final state relaxation and Madelung potential effects [25]. Bonnelle and co-workers have previously published an analysis of the $2p_{1/2}$ core level transition for CoO and Co_3O_4 compounds [26,27]. They deconvoluted the spectrum of Co $2p_{1/2}$ from Co_3O_4 into components with Co^{3+} in the octahedral coordination (oct) and Co^{2+} in the tetrahedral coordination (tet). According to their analysis, the Co^{2+}(tet) ion had a binding energy about 1.1 eV higher than the Co^{2+}(oct) for the CoO compound. We have also investigated two cobalt containing compounds for comparison, namely Co_3O_4 and $CoCl_2$. In the cobalt 2p spectrum of Co_3O_4, the separation Co $2p_{3/2}$–Co $2p_{1/2}$ was found to be 15.1 eV and a very weak satellite was observed at about 10 eV above the main Co 2p transitions. In this compound the presence of low-spin Co^{3+} ions is dominant, since the ratio Co^{3+} to Co^{2+} is 2:1, in agreement with a previous investigation of the same compound [24]. The Co 2p spectrum of $CoCl_2$ (see Fig. 3) shows satellite structure about 6 eV above the main Co 2p transition and the Co $2p_{3/2}$–Co $2p_{1/2}$ separation was found to be 16.0 eV. In this compound, cobalt is known to exist in a high-spin Co^{2+} state.

In the glass samples studied, the Co $2p_{3/2}$–Co $2p_{1/2}$ separation varied between 15.9 and 16.0 eV over the glass composition range investigated but this lies within the $< \pm 0.2$ eV error in determination of the binding energy. Furthermore, the strong satellite peaks about 5.6 eV above the main Co 2p lines, and the absence of any satellite structure in the region 10 eV above the core level lines, can clearly be seen for the data in Fig. 2. These observations confirm that cobalt, in the glass samples studied, exists in the high-spin Co^{2+} state. Since cobalt can also exist in both tetrahedral and octahedral coordination sites simultaneously [28], the Co 3p spectra were also measured to determine if such coordinations were present. Each Co 3p peak was resolved into two separate components and, using the same reasoning as Bonnelle et al. [26,27], the peak at higher binding energy is attributed to the contribution to Co 3p from high-spin Co^{2+} in tetrahedral coordination, while the peak at lower binding energy is due to high-spin Co^{2+} in octahedral coordination. Attempts to fit the Co 3p peak to one component only led to unacceptably large values of FWHM and thus this possibility was rejected. Fig. 10 shows the fitting of the Co 3p spectrum for the $x = 0.132$ glass, and the proportions of the different coordination geometries in each glass sample are given in Table 3. The large and small binding energy peaks could possibly be assigned to contributions from the Co^{2+} and the Co^{3+}, however, if this assignment is assumed, the calculated number of non-bridging oxygens present in the glass would be too large compared with the experimentally deduced number. In the case of the $x = 0.182$ glass, for example, the calculated percentage of non-bridging oxygens present, assuming a mixture of oxidation states, was found to be 86%, while the measured value was found to be 67% for the same sample — close to the 65.1% calculated for Co^{2+} only.

The O 1s spectra for the glass samples are shown in Fig. 5. A deconvolution method, similar to the one used to fit the Co 3p spectra, was used to fit each spectrum with contributions from both the bridging and non-bridging oxygen atoms. Fig. 11 shows a two

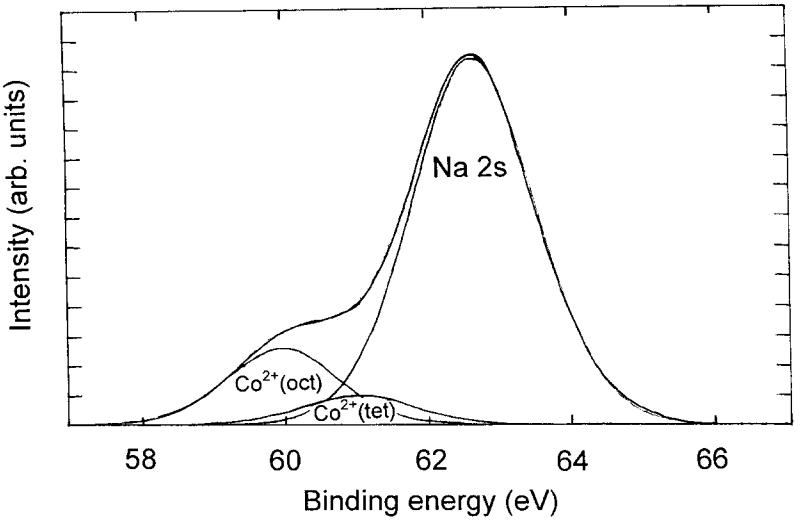

Fig. 10. A two peak fit of the Co 3p spectrum for the $x = 0.186$ glass, showing the contribution from Co^{2+}(oct) and Co^{2+}(tet).

peak fit for the $x = 0.132$ glass sample. Similar fittings were also obtained for the other glass compositions, although not shown here, and the non-bridging to total oxygen ratio was determined from the area ratios (area of non-bridging oxygen/area of total oxygen atoms) from the O 1s spectra. As can be seen from Fig. 11, the two Gaussian–Lorentzian sum function provides a good fit to the experimental data. The results of the fitting of the experimental O 1s spectra are summarised in Table 4. Previous studies have established that the experimental ratio of non-bridging to total oxygen in $0.70SiO_2$–$0.30Na_2$%O glass is ~38%, in excellent agreement with our findings [7]. If the cobalt, irrespective of its coordination state, is to behave as a network modifier, two non-bridging oxygen atoms must be formed, for every CoO molecule that is added to the glass.

Table 3
Binding energies and measured proportions of Co^{2+}(tet) and Co^{2+}(oct) in cobalt sodium silicate glasses. The numbers in parentheses represent the FWHM

x	Co^{2+}(oct) ±0.2eV	Co^{2+}(tet) ±0.2eV	Co^{2+}(oct)/Co^{2+}_{Total} ±10%
0.043	–	60.6 (1.9)	0
0.086	59.9 (1.9)	60.8 (1.9)	54
0.132	59.9 (1.9)	61.0 (1.9)	72
0.186	60.0 (1.9)	61.0 (1.9)	77

Consequently, the fraction of non-bridging oxygen should be given by

$$\text{NBO/Total Oxygen} = \frac{2[Na_2O] + 2[CoO]}{[Na_2O] + 2[SiO_2] + [CoO]}. \quad (1)$$

There is good agreement between Eq. (1) and the measured proportions of non-bridging oxygen atoms, as seen from Table 4, showing that Co^{2+}(tet) and Co^{2+}(oct) are both contributing to the non-bridging oxygen signal.

The changes in fitting parameters of the O 1s transitions, as CoO is substituted for SiO_2 in the glass structure, are shown in Fig. 12. The addition of CoO results in a decrease in the energy difference between the bridging and non-bridging oxygen peaks from 1.9 to 1.5 eV, and although the full width half maximum of the bridging oxygen peak does not appear to change much, that of the non-bridging oxygen does show ~30% increase, confirming that the unit SiOCo(II) is contributing to the non-bridging oxygen signal, but that it differs from the SiONa unit.

To investigate the effect of these two different non-bridging units, combinations of peaks were used to *simulate* the experimental spectra, based on the chemical units present in the glass. In this method, the ratio Z/r for the ion bonded to oxygen was used

as a crude measure of its ability to remove charge from the oxygen and thus increase the O 1s binding energy. Z is the nominal charge on the ion and r is its radius in nanometres, thus giving Z/r values of Si^{4+} (100), Na^{+} (9.8) and Co^{2+} (22.9). These numbers can be used to derive the values for the O 1s binding energy of the SiOCo(II) configuration by linear interpolation between the observed values for SiOSi and SiONa (from the base glass). This interpolation predicts that, as cobalt oxide is substituted for SiO_2, the O 1s signal from SiOSi at 531.5 eV would gradually be replaced by a peak from SiOCo(II) at a binding energy of approximately 530.3 eV, while the SiONa peak would remain at 529.6 eV. Fig. 11b shows the simulation based on the above model, using Gaussian–Lorentzian functions. The half widths of the peaks were fixed at the values taken from the base glass sample and the intensities obtained from the chemical composition. The simulation shown in Fig. 11b is for the base glass doped

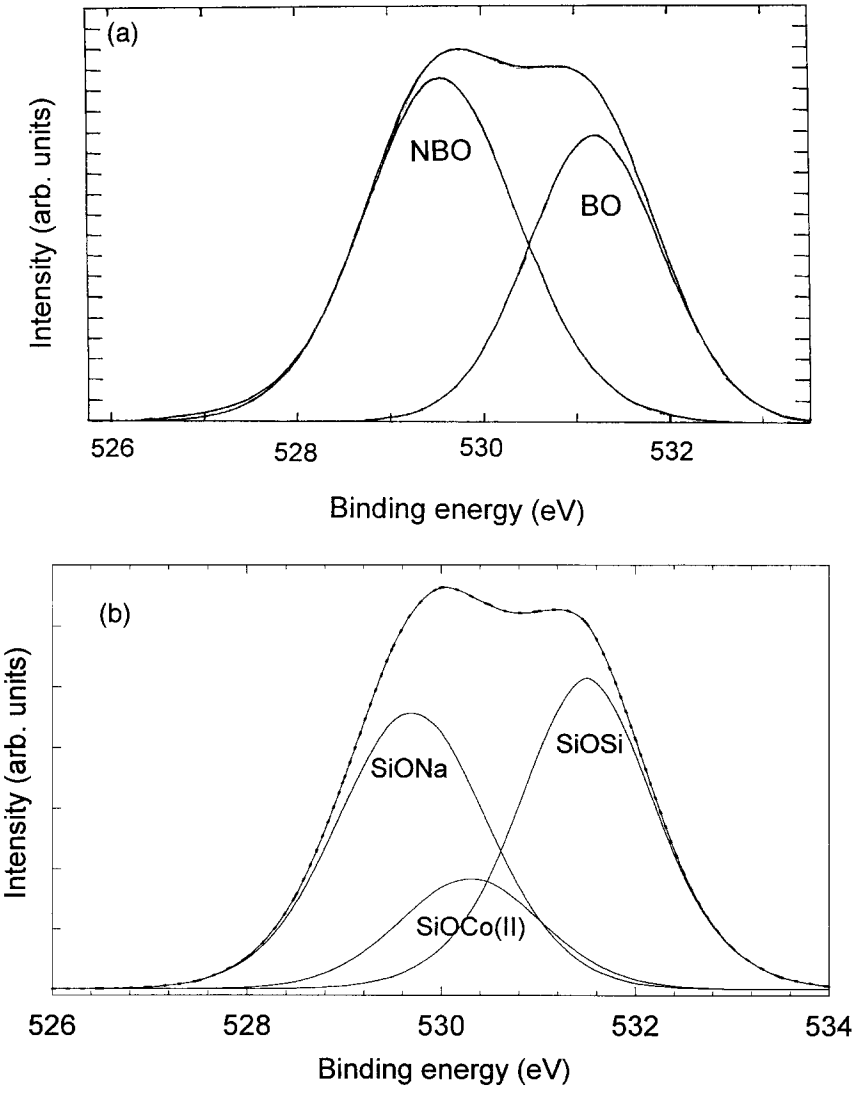

Fig. 11. (a) A two peak fit of the $x = 0.132$ glass, showing the contribution from BO and NBO. (b) A three peak fit of the $x = 0.132$ glass, showing contributions from SiOSi, SiONa and SiOCo.

Table 4
Measured and calculated (from Eq. (1)) proportions of non-bridging (NBO) to total oxygen (TO) in the cobalt sodium silicate glasses as a function of x

x	NBO/OT (%) measured ±5%	NBO/OT (%) calculated
0.0	38	36
0.043	41	41.4
0.086	50	48.4
0.132	58	57.2
0.186	67	65.1

with 13.2 mol% CoO. It is clear that this simple model reproduces the experimental data, for the glasses shown, at least as well as the two peak fit. The same was also true for the compositions not shown here. It was therefore possible, from the XPS data and modelling, to separate all the possible contributions to the non-bridging oxygen signal.

The increase in the non-bridging oxygen atoms in the glasses also results in an increase of those silicon atoms linked to non-bridging oxygen and hence, the Si 2p core level peak shifts to a lower binding energy with increasing CoO content. Similar behaviour has also been observed in previous studies of Na–Fe [14] and Na–Ca [29] silicate based glasses. However, the Na 1s spectra are somewhat insensitive

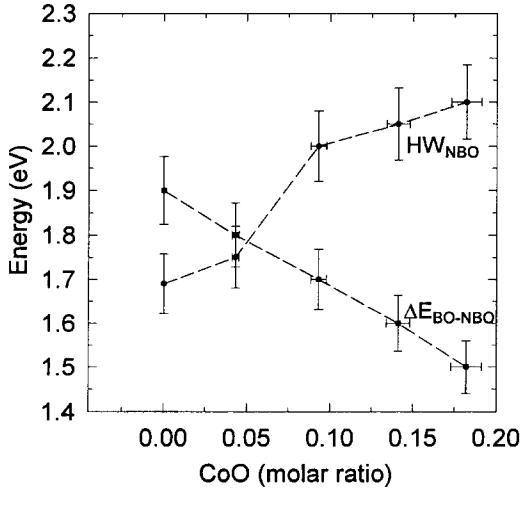

Fig. 12. Variation of the fitting parameters for the O 1s spectra vs. CoO content. HW_{NBO} is the half width of the non-bridging oxygen signal, while ΔE_{BO-NBO} is the separation between bridging oxygen and non-bridging oxygen transitions.The dashed lines are drawn as guides for the eye.

Table 5
Binding energies for the core levels Si 2p and Na 1s; in parentheses are the FWHM values

x	Si 2p (eV) ±0.2 eV	Na 1s (eV) ±0.2 eV
0.0	102.0 (1.95)	1071.5 (2.0)
0.046	101.9 (2.2)	1071.5 (2.2)
0.086	101.6 (2.2)	1071.4 (2.3)
0.132	101.4 (2.1)	1071.1 (2.1)
0.186	101.0 (2.1)	1070.9 (2.1)

to changes in CoO content in the glasses. A change in peak position (as seen from Table 5) and no change in the peak shape or peak width indicates that the sodium atoms exist in the same chemical environment over the glass composition range studied.

4.2. Physical property data

The physical properties of the series of glass samples are summarized in Fig. 6. The density of the glass increases linearly with increasing CoO content. This behaviour is expected because the density of CoO is higher than that of SiO_2. The glass transition temperature and the thermal expansion coefficient, both decrease with increasing CoO in the glass. A decrease in T_g is indicative that CoO is entering the glass as a network modifying ion, although an increase in α might also be expected.

4.3. Magnetization results

The Curie temperature, θ_p, is a measure of the strength of the magnetic ion–ion interaction and therefore, the larger $|-\theta_p|$, the stronger is the interaction. The negative Curie temperature indicates that the exchange interaction is antiferromagnetic. As seen from Table 6, θ_p is negative for all the glasses

Table 6
Parameters derived from the data χ^{-1} versus temperature for the cobalt sodium silicate glasses

x	Co ions/g 10^{20} ±5%	C (emu K/g) 10^{-3} ±5%	$-\theta_p$ (K) ±1%	μ_{eff} (BM)
0.043	4.2	2.4	2.8	5.22
0.086	8.3	4.7	8.7	5.2
0.132	12.7	7	12.8	5.15
0.186	17.6	9.6	18.5	5.12

indicating that cobalt is behaving antiferromagnetically and since $|-\theta_p|$ is increasing, the interaction becomes stronger with increase in CoO in the glasses. The increase in the exchange interaction is also confirmed by the scaling argument represented in Fig. 9a–d. Comparing the four sets of curves, we observe increasing divergence of the data on the H/T scale with increase in CoO. The data collapses to a single universal curve for the smallest CoO concentration only (Fig. 9a). The non-collapsing of the M vs. H/T curves at larger CoO concentration is seen as evidence of increasing antiferromagnetic exchange interaction, which is also seen in the increase of $|-\theta_p|$. Similar behavior has been seen in lead borate glasses when increasing amounts of Fe_2O_3 are incorporated in the glasses [30]. However, in the case of silicate glasses doped with various amounts of CuO [15], it was found that the data on the H/T scale collapsed completely to a single curve indicating that the copper in the glass structure was behaving paramagnetically. It should also be noted that the theoretical value for the magnetic moment for Co^{2+}(tet) is 4.5 μ_B, while for Co^{2+}(oct) it is 5.1 μ_B [31]. The values for the effective magnetic moment in our glass samples were in the range 5.18 ± 0.2 μ_B indicating the presence of octahedral high-spin Co^{2+} only in these glass samples.

5. Conclusions

XPS and magnetization techniques have been used to study the effect, on the structural and magnetic properties, of introducing various amounts of CoO in sodium silicate based glass. The XPS data suggest that cobalt exists as high spin Co^{2+}(tet) and Co^{2+}(oct) simultaneously in all the cobalt doped glass samples but the magnetisation data shows evidence for the octahedral coordination only. Since XPS is sampling only the first few nanometres of the surface, this difference may indicate that the preferred coordination for Co^{2+} in the bulk glass is octahedral (typical of a modifier) but the surface reconstruction of the glass structure forces some Co^{2+} into a tetrahedral environment. The O 1s spectra have been fitted with contributions from both bridging and non-bridging oxygen atoms, and the non-bridging oxygen signal was found to increase with increase in CoO content, indicating that cobalt is behaving as a network modifier. The measured physical properties confirmed these findings. The magnetization curves plotted as a function of H/T show a divergence in the data which increases with increasing CoO content indicating that the exchange interaction between the magnetic ions also increases with increasing amount of CoO. From the Curie temperature, it has also been shown that the exchange interaction is antiferromagnetic in this series of glasses.

References

[1] McIntyre, M.G. Cook, Anal. Chem. 47 (1975) 2208.
[2] S. Huffner, G.K. Wertheim, Phys. Rev. B8 (1973) 4857.
[3] D.C. Frost, C.A. McDowell, J.S. Woolsey, Molec. Phys. 27 (1974) 1473.
[4] A. Mosser, M.A. Romeo, J.C. Parlebas, K. Okada, A. Kotani, Solid State Commun. 79 (1991) 641.
[5] C.G. Pantano, in: Experimental Techniques of Glass Science (American Ceramic Society, Westerville, OH) p. 129.
[6] R. Gresch, W. Muller-Warmuth, J. Non-Cryst. Solids 34 (1979) 127.
[7] B.M.J. Smets, T.M.P. Lommen, J. Non-Cryst. Solids 46 (1981) 21.
[8] S. Mukhopadhyay, S.H. Garofalini, J. Non-Cryst. Solids 126 (1990) 202.
[9] P.I.K. Onorato, M.N. Alexander, C. Struck, G.W. Tasker, D.R. Uhlmann, J. Am. Ceram. Soc. 68 (1985) 148.
[10] B.M.J. Smets, D.M. Krol, Phys. Chem. Glasses 25 (1984) 113.
[11] C.H. Hsieh, H. Jain, A.C. Miller, E.I. Kamitsos, J. Non-Cryst. Solids 168 (1994) 247.
[12] R.K. Brow, R.J. Kirkpatrick, G.L. Turner, J. Am. Ceram. Soc. 73 (1990) 2293.
[13] Z. Hussain, M.A. Salim, M.A. Khan, E.E. Khawaja, J. Non-Cryst. Solids 110 (1989) 127.
[14] A. Mekki, D. Holland, C.F. McConville, M.A. Salim, J. Non-Cryst. Solids 208 (1996) 267.
[15] A. Mekki, D. Holland, C.F. McConville, J. Non-Cryst. Solids 215 (1997) 271.
[16] R.K. Brow, C.M. Arens, X. Yu, E. Day, Phys. Chem. Glasses 35 (1994) 132.
[17] M.A. Salim, G.D. Khattak, M.S. Hussain, J. Non-Cryst. Solids 185 (1995) 101.
[18] J.S. Brinen, in: Applied Surface Analysis, ed. T.L. Barr and L.E. Davis (American Society for Testing Materials, Pittsburgh, PA, 1978) p. 24.
[19] K. Moorjani, J.M.D. Coey, Magnetic Glasses (Elsevier, Amsterdam, 1984).

[20] E.E. Khawaja, Z. Hussain, M.S. Jazzar, O.B. Daboussi, J. Non-Cryst. Solids 93 (1987) 45.
[21] B.M.J. Smets, T.P.A. Lommen, J. Am. Ceram. Soc. 65 (1982) C80.
[22] L.F. Olfield, Glass Technol. 6 (1964) 41.
[23] D. Briggs, V.A. Gibson, Chem. Phys. Lett. 25 (1974) 493.
[24] T.J. Chuang, C.R. Brundle, D.W. Rice, Surf. Sci. 59 (1976) 413.
[25] K. Wandelt, Surf. Sci. Rep. 2 (1982) 1.
[26] J.P. Bonnelle, J. Grimblot, A. D'Huysser, J. Electron Spec. 7 (1975) 151.
[27] J. Grimblot, A. D'Huysser, J.P. Bonnelle, J.P. Beaufils, J. Electron Spec. 6 (1975) 71.
[28] E. Baiocchi, A. Montenero, M. Bettinelli, J. Non-Cryst. Solids 46 (1981) 203.
[29] B.W. Veal, D.J. Lam, A.P. Paulikas, J. Non-Cryst. Solids 49 (1982) 309.
[30] S.K. Mendiratta, M.A. Valente, J.A.A.J. Perenboom, J. Non-Cryst. Solids 134 (1991) 100.
[31] F.A. Cotton, G. Wilkinson, Advanced Inorganic Chemistry (Wiley, New York, 1966).